Interfacial Mechanisms Of Cationic And Anionic Emulsifiers In Asphalt Emulsions

Jing Hu[1] and Senlin Gao[2*]

[1] School of Engineering Management, Zhengzhou University of Economics and Business, He'nan Zhengzhou, 451191, China
[2] School of Civil Engineering, Chongqing Jiaotong University, Chongqing, 400074, China
[*] Corresponding author. E-mail: forest@mails.cqjtu.edu.cn

Received: Feb. 03, 2026; Accepted: Apr. 23, 2026

This study investigates the interfacial characteristics and stabilization mechanisms of anionic emulsifiers (KDS and SDBS) and cationic emulsifiers (STAC and STAB) in asphalt emulsions through interfacial tension analysis, storage stability testing, and molecular dynamics (MD) simulations. The results demonstrate that cationic systems exhibit superior performance; STAC and STAB reduced interfacial tension by 63.6% and 62.6%, respectively, significantly outperforming the anionic systems (50.8% and 47.3%). Furthermore, cationic systems maintained 5-day storage separation rates below 5%, whereas anionic systems exceeded 13%. MD simulations elucidated that cationic emulsifiers form dense interfacial monolayers through robust electrostatic interactions, characterized by an interfacial energy of -85kcal/mol and an aggregation peak of 13.26. Notably, electrostatic forces accounted for more than 65% of the total interaction energy in cationic systems. In contrast, anionic emulsifiers exhibited loose adsorption patterns due to electrostatic repulsion, resulting in a higher interfacial energy of -70kcal/mol. Hydrophilic-lipophilic balance (HLB) analysis further confirmed optimal values for cationic surfactants, whereas KDS exhibited excessive hydrophilicity. All experiments were conducted under standard conditions (60°C for interfacial tension measurement, 25°C for storage stability testing, and pH 7.0). These findings provide fundamental molecular-level insights for the design of high-performance emulsified asphalt.

Keywords: Emulsified asphalt; Emulsifier; Oil-water interface; Molecular dynamics; Stability

http://dx.doi.org/10.6180/jase.202609_32.048

1. Introduction

Emulsified asphalt serves as a cornerstone of modern pavement preservation, extensively utilized in applications such as micro-surfacing, fog sealing, slurry sealing, pavement recycling, and thin overlays [1]. Its widespread adoption is driven by significant advantages over traditional hot-mix asphalt, including a mitigated environmental footprint, enhanced construction safety, and reduced operational costs, all while extending pavement service life [2, 3]. By enabling production, application, and compaction at ambient temperatures, emulsified asphalt facilitates the energy-efficient treatment of various pavement distresses, ranging from longitudinal and transverse cracking to routine maintenance of high-grade roadways [4, 5]. However, despite its substantial potential for sustainable infrastructure development, the inadequate interfacial stability within emulsified asphalt systems remains a primary technical bottleneck, hindering broader application and long-term performance reliability.

As a complex oil-in-water (O/W) system, emulsified asphalt is produced by mechanically dispersing molten asphalt into an aqueous phase containing specialized surfactants [6]. The physicochemical properties of the resulting oil-water interface are governed by a synergy of factors, including asphalt composition, emulsifier type and

concentration, pH, and temperature [7–10]. Previous research indicates that cations enhance emulsion stability by reinforcing the electrical double layer surrounding the asphalt droplets, thereby preventing particle agglomeration [11]. Specifically, maintaining Na^+ concentrations below 0.1 wt% typically ensures favorable stability, while the incorporation of nanoparticles has been shown to improve dynamic stability and refine droplet size [12]. Furthermore, monovalent cations can augment adsorption strength at the interface by modulating the hydrophilicity of surfactants such as SDBS [13]. However, stability deteriorates when cation concentrations exceed critical thresholds (e.g., 5 wt% for SDS and 4 wt% for KDS), as electrostatic attraction triggers the migration of emulsifier molecules from the interface into the bulk aqueous phase [14]. The heating and annealing treatment of asphalt promotes the aggregation of honeycomb structures, which is manifested in the reduction of the spacing between honeycomb structures and the formation of more and smaller honeycomb structures [15]. Molecular architecture also plays a pivotal role in interfacial integrity. Emulsifiers featuring long alkyl chains can form robust hydration layers through hydrogen bonding with water molecules, creating microphase structures that bolster stability. The lipophilicity of these long-chain groups promotes dense adsorption toward the asphalt phase, thickening the interfacial film and reducing interfacial tension by over 90% [16]. The addition of phenyl groups or the use of specific isomers, such as the para-isomer of SDBS ($4-1\Phi C12S$), further enhances the protective barrier at the asphalt-water interface [16, 17]. Similarly, long-chain Gemini surfactants and short-chain variants with C_4 spacers have demonstrated the capacity to significantly lower interfacial tension even at low dosages [18, 19].

Despite these extensive investigations into macroscopic variables such as emulsifier type and ionic concentration, a fundamental understanding of the interfacial microstructure and the underlying intermolecular stabilization mechanisms remains elusive. Existing literature relies heavily on macroscopic performance characterization, which lacks direct visualization of molecular behavior at the interface. Furthermore, the individual contributions of diverse intermolecular forces—including electrostatic interactions, hydrogen bonding, and van der Waals forces—to overall interfacial stability have not been sufficiently quantified.

MD simulations offer a robust theoretical framework that complements experimental observations by enabling high-resolution analysis of the spatial arrangement and orientation of emulsifier molecules at the oil-water interface [17]. This approach facilitates the direct visualization and quantification of fundamental interfacial interactions, including hydrogen bonding, electrostatic forces, and van der Waals interactions [18]. Previous studies utilizing MD have demonstrated that cationic asphalt emulsions formulated with octadecyl trimethyl ammonium chloride develop a wider oil-water transition region and a thicker interfacial film, both of which are critical for enhancing storage stability [19]. Similarly, increasing concentrations of SDBS lead to the formation of a well-defined interfacial boundary layer, effectively extending oil-water separation times [20]. Furthermore, complex interactions such as cation-π forces between aromatic systems and metal ions have been shown to influence local accumulation at the interface, with the affinity of heavy metals for bituminous materials following the hierarchy: $Cr > Pb > Ni > Cd > Cu > Zn$ [21].

Despite these advancements, systematic investigations that integrate experimental validation with molecular-level simulations to elucidate the relationship between emulsifier chemical structure and interfacial performance remain scarce. To address this knowledge gap, the present study comprehensively evaluates the interfacial characteristics and stabilization mechanisms of two anionic (KDS, SDBS) and two cationic (STAC, STAB) emulsifiers. Through a combination of interfacial tension analysis, storage stability testing, and MD simulations, this research quantifies the interfacial energy, adsorption density, and the relative contribution of various intermolecular forces. The findings provide a molecular-level blueprint for the design of high-performance emulsified asphalt systems optimized for rapid road repair applications.

This study integrates experimental characterization with MD simulations to systematically elucidate the interaction mechanisms between Asphalt, emulsifier molecules, and the aqueous phase at the oil-water interface. By bridging microscopic molecular behavior with macroscopic performance metrics, this research establishes a theoretical framework for the rational design of high-performance emulsified asphalt.

2. Experimental setup

2.1. Experimental Materials

In this study, a 70# penetration grade asphalt was selected as the base binder for the preparation of the asphalt emulsions. The fundamental physical properties of the 70# asphalt were evaluated in accordance with the Chinese standard JTG E20-2011, with the results summarized in Table 1. To further characterize the chemical composition, the asphalt's four fractions (Saturates, Aromatics, Resins, and Asphaltenes; SARA) were quantified using Thin-Layer Chromatography-Flame Ionization Detection (TLC-FID)

Table 1. Main technical indicators of 70# base asphalt

Experimental Indicators	Penetration (0.1 mm, 15°C)	Softening point (°C)	Ductility (cm, 15°C)
Experimental results	65.7	47.9	152
Experimental Requirements	60–80	43–46	> 100

Table 2. Proportion of the four components of 70# base asphalt (%)

Asphalt Type	asphaltene	gelatinous	Aromatic fraction	Saturation fraction
70#	12.44	26.62	44.62	16.32
Experimental Requirements	> 10	31–55	21–47	12–27

[22]. The raw data from the TLC-FID system were processed and analyzed using the integrated SIC-4800II software, and the resulting fractional distributions are reported in Table 2.

Four distinct surfactants were selected to investigate the influence of ionic charge and molecular structure on emulsion stability: two anionic emulsifiers, KDS and SDBS; and two cationic emulsifiers, STAC and STAB. To ensure the reliability and reproducibility of the experimental results, all emulsifiers were of analytical grade and sourced from Shanghai Aladdin Biochemical Technology Co., Ltd. The use of high-purity surfactants minimizes the interference of impurities on interfacial tension measurements and molecular dynamics simulations. The fundamental physicochemical properties of these emulsifiers, including molecular weight and chemical formula, are summarized in Table 3.

Asphalt emulsions with a 50% residue (solid content) were fabricated using a laboratory-scale colloid mill (Herbert Rink GmbH, Germany). To ensure optimal storage stability and interfacial performance, the emulsifier dosage was maintained at 3.0% by total weight of the emulsion [17]. The systematic preparation protocol is depicted in Figure 1.

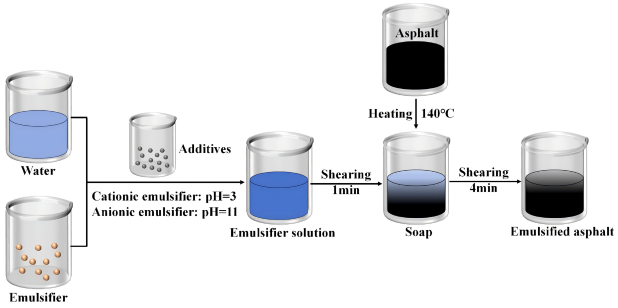

Fig. 1. The preparation process of emulsified asphalt

2.2. Surface Tension and Interfacial Tension Measurements

Surface tension and interfacial tension are critical parameters for evaluating surfactant efficiency. Surface tension reflects the air-water interfacial activity of emulsifier solutions, while oil-water interfacial tension directly quantifies the energy reduction at the asphalt-water boundary, which governs droplet formation and emulsion stability.

In this study, both surface tension and asphalt-water interfacial tension were measured using a Dataphysics DCAT21 tensiometer equipped with the Wilhelmy plate method for surface tension and the Du Noüy ring method for interfacial tension. For surface tension measurements, emulsifier solutions (3.0 wt%) were equilibrated at 25°C. For interfacial tension measurements, the asphalt phase was heated to 60°C to maintain fluidity, and measurements were conducted at the interface between the molten asphalt and the aqueous emulsifier solution at 60°C. Each measurement was repeated at least three times, with results reported in millinewtons per meter (mN/m).

2.3. Storage Stability Test

The storage stability of emulsified asphalt signifies its ability to maintain a uniform dispersion of Asphalt droplets within the aqueous phase over time, resisting physical or chemical changes such as sedimentation, flocculation, and coalescence [23]. In this study, the storage stability was evaluated in accordance with the JTG E20-2011 T0655 standard.

2.4. Laser particle size analysis method for emulsified asphalt

The stability of an asphalt emulsion is fundamentally governed by the orientation of surfactant molecules at the oil-water interface. The hydrophobic tails of the emulsifiers adsorb onto the Asphalt surfaces, while the hydrophilic head groups extend into the continuous aqueous phase, forming a protective barrier that inhibits droplet coalescence and aggregation. In this system, a smaller average particle size typically correlates with superior emulsification efficiency and enhanced kinetic stability. The testing procedure is as follows:

1. Dilute the emulsion with distilled water at a ratio of

Table 3. Properties of emulsifiers

Emulsifier	Molecular formula	Molecular weight(g/mol)	CAS
KDS	$C_{12}H_{25}SO_4$ K	300.48	23329-35-7
SDBS	$C_{18}H_{29}SO_3Na$	348.48	25155-30-0
STAC	$C_{21}H_{46}NCl$	348.05	112-03-8
STAB	$C_{21}H_{46}NBr$	393.50	1120-02-1

1:100.

2. Add the diluted emulsified asphalt to the sample cell of the laser particle size analyzer.

3. Activate the circulation system and initiate particle size measurement once the sample achieves a uniform distribution state.

2.5. Construction and Validation of Asphalt Models

Asphalt is a chemically complex mixture comprising organic molecules with diverse molecular weights, polarities, and functional groups [24]. To capture this complexity, this study utilized a refined twelve-molecule, four-component model to represent the asphaltene, resin, aromatic, and saturate fractions [25]. This multicomponent model has been widely validated for its ability to accurately replicate the fundamental physicochemical properties of natural Asphalt, including density, thermal expansion coefficients, rheological behavior, and mechanical performance [26, 27].

The chemical structures of the representative molecules within this twelve-component binder model are illustrated in Figure 2. To ensure the simulation results were directly comparable to the laboratory findings, the relative proportions of these molecules were specifically adjusted to align with the SARA fraction distribution of the 70# base asphalt determined via TLC-FID (as reported in Table 2). This tailored approach allows for a high-fidelity representation of the specific binder used in the experimental phase, providing a robust basis for exploring the interfacial interactions with the selected emulsifiers.

Comprehensive details regarding the molecular structures, stoichiometric ratios, and chemical formulas of the individual molecules within the asphalt model are provided in Table 4. The resulting three-dimensional configuration of the equilibrated asphalt binder is illustrated in Figure 3.

To achieve a stable, low-energy state, the constructed molecular system underwent a rigorous multi-step equilibration protocol. Initial geometric optimization was performed to eliminate high-energy overlaps between atoms. Subsequently, an annealing procedure-comprising 30 cycles across a temperature range of 300 K to 500 K-was implemented to overcome local energy barriers and ensure a realistic spatial distribution of the SARA fractions.

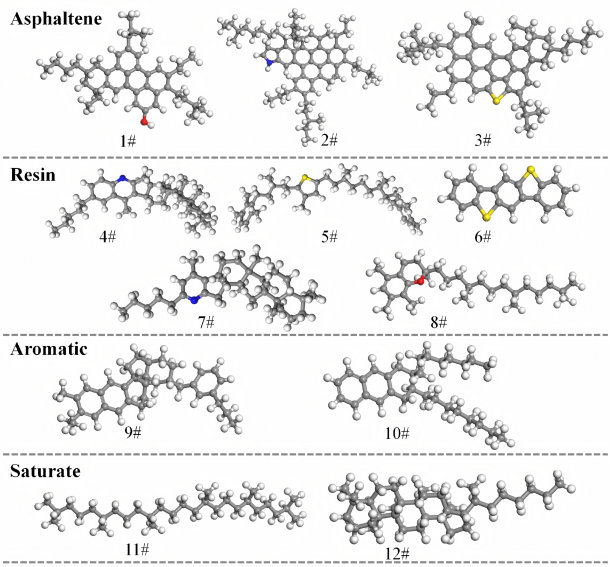

Fig. 2. Asphalt twelve-molecular model

The refined model was then subjected to a series of molecular dynamics runs using both isobaric-isosteric and canonical ensembles. Kinetic simulations were conducted for a duration of 200 ps to reach thermodynamic equilibrium. Long-range electrostatic interactions were computed using the high-precision Ewald summation method, while van der Waals forces were calculated via an atom-based summation algorithm with a defined cutoff distance. This systematic approach ensures that the density and cohesive energy density of the model align with experimental values, providing a robust baseline for subsequent interfacial analysis.

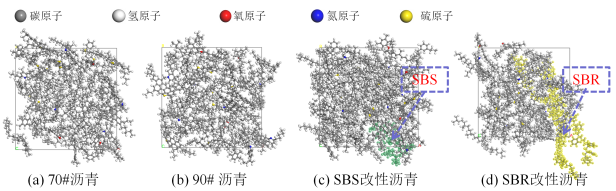

Fig. 3. Asphalt binder molecular model

Density serves as a fundamental parameter for characterizing the thermal stability and brittle-transition behavior of asphalt; consequently, it is frequently utilized as a

Table 4. The number of molecules added in the asphalt molecular model

Asphalt Components	Molecular Name	Molecular weight (g/mol)	Quantity	Simulated value (%)	Experimental value (%)
Asphaltic	phenol (1#), $C_{42}H_{54}O$	575.00	1	12.60	12.44
	pyrrole (2#), $C_{66}H_{81}N$	888.50	1		
	Thiophene (3#), $C_{51}H_{62}S$	707.20	1		
Resinous	Quinoline Phosphate (4#), $C_{40}H_{59}N$	554.00	2	26.98	26.62
	Isoprene (5#), $C_{40}H_{60}S$	573.10	1		
	Benzobenzothiophene(6#), $C_{18}H_{10}S_2$	290.40	4		
	Pyridine (7#), $C_{36}H_{57}N$	530.90	2		
	Trimethylphenoxane (8#), $C_{29}H_{50}O$	414.80	2		
Aromatic	Hydrogenated naphthalene (9#), $C_{35}H_{44}$	464.80	14	44.14	44.62
	Di-n-octyl cyclohexane-naphthalene (10#), $C_{30}H_{46}$	406.80	2		
Saturated	Squalane (11#), $C_{30}H_{62}$	422.90	4	16.32	16.32
	Hoxane (12#), $C_{35}H_{62}$	483.00	1		

benchmark to validate the structural integrity of molecular models [8]. Figure 4 illustrates the temporal evolution of the system's density during the equilibration process. For the 70# base asphalt binder, the model-predicted density was determined to be 0.965 g/cm^3, representing a marginal deviation of only 1.2% from the experimentally measured value of 0.993 g/cm^3. This discrepancy is well within the widely accepted relative error threshold established in literature for molecular dynamics simulations of bituminous materials [20]. These results confirm that the constructed twelve-molecule SARA model effectively replicates the physical characteristics of the actual binder, providing a high-fidelity foundation for the subsequent analysis of interfacial interactions.

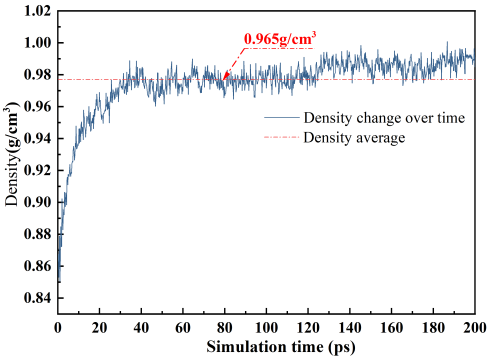

Fig. 4. Asphalt molecular model density change over time

2.6. Oil/Water Interface Model

To investigate the molecular aggregation and orientation behavior at the oil-water boundary, a multi-layer interface model was developed. The chemical structures of the four investigated surfactants—KDS, SDBS, STAC, and STAB—are illustrated in Figure 5, with water molecules represented using the high-precision TIP3P model. Following established methodologies [17, 28], an optimal emulsifier concentration of 15% within the aqueous phase was selected, equivalent to a 7.5% dosage relative to the total mass of the emulsified asphalt system.

The emulsifier solution models were subjected to a rigorous equilibration protocol, including geometric optimization, annealing cycles, and kinetic simulations, to achieve a stable potential energy minimum. The simulations were performed using the COMPASS force field, which is specifically optimized for organic and polymeric materials. Long-range electrostatic interactions were resolved using the Ewald summation method, while van der Waals forces were computed via an atom-based summation algorithm with a cutoff radius of 15.5 Å. This substantial cutoff distance ensures that the non-bonded interactions, critical for predicting interfacial tension and energy, are captured with high accuracy.

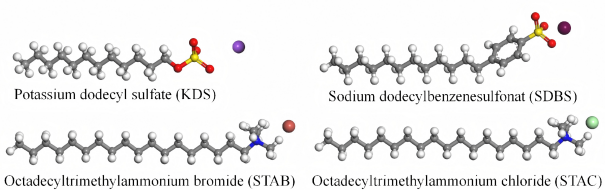

Fig. 5. Emulsifier molecular model

To mitigate the influence of periodic boundary artifacts and prevent unwanted interactions between periodic im-

ages in the z-direction, a 30 Å vacuum buffer layer was integrated atop the emulsifier solution phase. The resulting configuration of the asphalt-water-emulsifier interface model is depicted in Figure 6.

To ensure the elimination of any energetically unfavorable or sterically unrealistic structures, the composite interface model underwent a comprehensive refinement sequence involving geometric optimization, annealing cycles, and multi-stage kinetic simulations. The dynamic equilibration was executed in two distinct phases:

1. An initial 500 ps production run under the isobaric-isosteric ensemble to allow for system volume relaxation and density stabilization at the interface.
2. A subsequent 500 ps simulation under the canonical ensemble to ensure thermal equilibrium while maintaining a constant volume.

Consistent with the bulk system parameters, long-range electrostatic interactions were resolved via the Ewald summation method, while van der Waals forces were determined using an atom-based summation algorithm. This staged approach guarantees that the system reaches a stable state before data collection, providing a reliable basis for quantifying interfacial energy and molecular orientation.

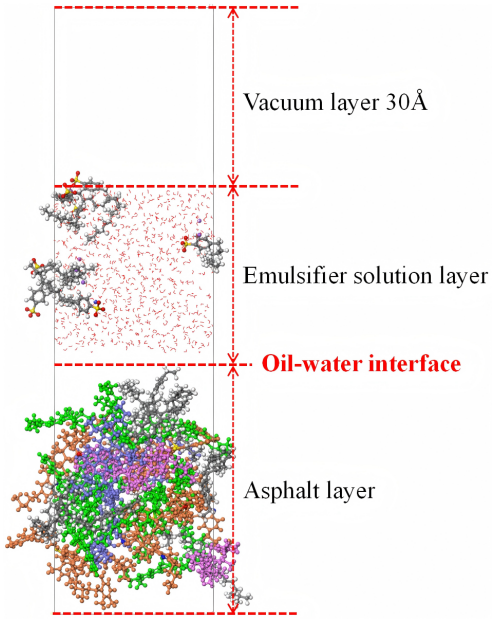

Fig. 6. Oil/Water Interface Model

3. Result discussions

3.1. Surface Tension and Interfacial Tension Results

Surface tension and asphalt-water interfacial tension were measured to comprehensively evaluate surfactant performance. Surface tension reflects the general interfacial activity at the air-water interface, while interfacial tension at the asphalt-water boundary directly relates to emulsification efficiency. Figure 7 presents the surface tension results for the four emulsifier solutions. All surfactants effectively reduced the surface tension of pure water (72.8 mN/m). Cationic emulsifiers exhibited superior surface activity; STAC and STAB reduced surface tension to 26.5 mN/m and 27.2 mN/m, respectively (63.6% and 62.6% reduction). Anionic emulsifiers showed comparatively lower reductions, with KDS reaching 35.8 mN/m (50.8% reduction) and SDBS reaching 38.4 mN/m (47.3% reduction). More importantly, Figure 7 presents the asphalt-water interfacial tension measurements, which directly govern emulsion droplet formation. The interfacial tension of asphalt against pure water was 38.5 mN/m. Cationic emulsifiers demonstrated markedly superior interfacial tension reduction: STAC and STAB lowered the asphalt-water interfacial tension to 8.2 mN/m and 8.6 mN/m, respectively (78.7% and 77.7% reduction). In contrast, anionic systems achieved only moderate reductions, with KDS reaching 15.3 mN/m (60.3% reduction) and SDBS reaching 14.1 mN/m (63.4% reduction). The correlation between interfacial tension and emulsion properties is evident: lower asphalt-water interfacial tension corresponds to smaller median particle sizes (Figure 9) and improved storage stability (Figure 8). Specifically, the cationic systems with interfacial tensions below 9 mN/m produced emulsions with median particle sizes of 2.1–2.3 μm, whereas anionic systems with interfacial tensions above 14 mN/m yielded larger particles (6.2–7.4 μm). This relationship confirms that asphalt-water interfacial tension serves as a reliable predictor of emulsification performance.

This variation stems from the distinct adsorption mechanisms of different emulsifier types at the interface. The quaternary ammonium group ($-N^+(CH_3)_3$) of cationic emulsifiers exhibits strong electrostatic attraction with negatively charged polar components in asphalt (e.g., carboxyl and phenolic hydroxyl groups in asphaltenes), promoting their oriented arrangement at the oil-water interface. Simultaneously, the C_{18} long-chain alkyl group penetrates the oil phase, forming a tightly ordered monolayer. This dual mechanism of head-group anchoring and tailchain insertion ensures the compactness and stability of the interfacial film. In contrast, the sulfonate groups ($-SO_3^-$) of anionic surfactants exhibit electrostatic repulsion with negatively charged asphalt components, weakening interfacial adsorption strength. Furthermore, the shorter C_{12} alkyl chain of KDS results in weaker hydrophobic interactions. Although SDBS contains a benzene ring structure, its over-

all interfacial activity remains lower than that of cationic systems.

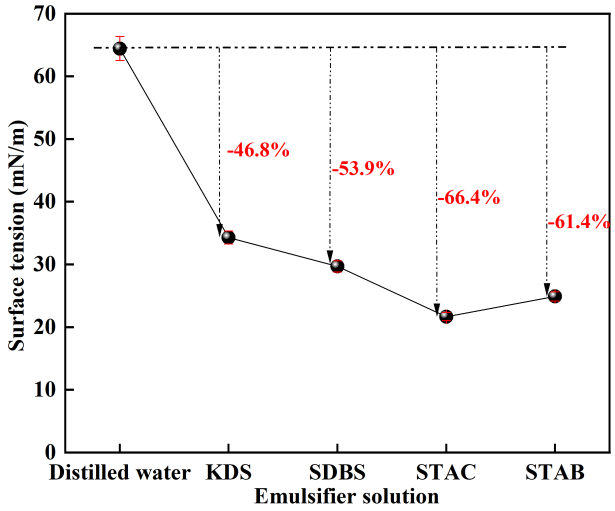

Fig. 7. Surface tension of emulsifier aqueous solution

The HLB is a critical semi-empirical parameter that quantifies the relative affinity of a surfactant for the aqueous and oil phases. The HLB value dictates the functional application of the emulsifier: values between 1 and 6 indicate lipophilic dominance, suitable for water-in-oil (W/O) systems, while the range of 7 to 9 represents a transitionary balanced character. Surfactants with HLB values between 8 and 18 are predominantly hydrophilic, rendering them ideal for stabilizing oil-in-water (O/W) emulsions, such as the asphalt systems investigated here. Beyond an HLB of 18, the molecules exhibit extreme hydrophilicity, which is generally used for solubilizing water-insoluble substances. In this study, the HLB values of the selected emulsifiers were evaluated to correlate their chemical structures with their observed emulsification efficiency. While the cationic surfactants (STAC and STAB) fell within the optimal range for O/W stability, the anionic emulsifier KDS exhibited an HLB exceeding the ideal threshold. This excessive hydrophilicity likely weakens its adsorption at the asphalt interface, as the molecule prefers the bulk aqueous phase, thereby contributing to the higher separation rates observed in the laboratory storage stability tests. The HLB value is calculated as follows:

$$HLB = 7 \times \sum H_{\text{hydrophilic}} - \sum L_{\text{lipophilic}} \quad (1)$$

In the formula: $H_{\text{hydrophilic}}$ is the weighting factor for the hydrophilic group, and $L_{\text{lipophilic}}$ is the weighting factor for the lipophilic group.

The HLB values of the emulsifier molecules are shown in Table 5. The HLB values of each emulsifier vary significantly, reflecting their structural differences and affecting their interfacial behavior in asphalt emulsion systems. KDS exhibits a calculated HLB value of 40, indicating strong hydrophilicity stemming from the highly hydrophilic sulfonate group ($-SO_3^-$) and its relatively short C_{12} alkyl chain. An excessively high HLB (> 20) causes the emulsifier to preferentially remain dispersed in the aqueous phase rather than adsorb at the asphalt-water interface, resulting in poor interfacial coverage and reduced emulsification efficiency. SDBS possesses a calculated HLB value of 18. Although it shares a sulfonate hydrophilic group with KDS, its aromatic benzene ring and longer C_{18} alkyl chain provide enhanced lipophilicity, resulting in a more balanced hydrophilic-lipophilic ratio. However, the molecule remains predominantly hydrophilic (HLB > 15), which still limits its effectiveness for asphalt-in-water emulsions compared to more balanced surfactants.

Table 5. The HLB value of the emulsifier

Emulsifier	$\sum H_{\text{hydrophilic}}$	$\sum H_{\text{lipophilic}}$	HLB
KDS	38.7	5.7	40
SDBS	19.1	8.057	18.025
STAC	9.40	8.55	7.85
STAB	9.40	8.55	7.85

Conversely, the cationic emulsifiers (STAC and STAB) exhibit calculated HLB values of approximately 7.9, which aligns more closely with the optimal HLB range (8.0-8.5) for stable asphalt-in-water dispersions in this study. The quaternary ammonium group ($-N^+(CH_3)_3$) provides moderate hydrophilicity, while the C_{18} longchain alkyl group offers sufficient lipophilicity. This more balanced amphiphilicity ensures effective partitioning to the oil-water interface and formation of a protective adsorption layer. Importantly, counterion type (chloride in STAC vs. bromide in STAB) exerts negligible influence on HLB values, as expected from HLB theory.

3.2. Storage Stability of Emulsified Asphalt

The 5-day storage stability results for the various emulsified asphalt formulations are presented in Figure 8. As asphalt emulsions are inherently thermodynamically unstable systems, the separation rate for all formulations increased progressively with extended storage time. This phenomenon is driven by the density differential between the asphalt droplets and the aqueous phase, which triggers gravitational sedimentation over time. However, cationic emulsified asphalt demonstrated superior storage stability. The STAC system exhibited separation rates of 1.2%, 2.8%, and 4.5% at 1, 3, and 5 days, respectively, while the STAB system showed 1.3%, 3.1%, and 4.8%. Both systems main-

tained separation rates below the 5% technical requirement at 5 days. In contrast, anionic emulsified asphalt demonstrated relatively poorer stability: the KDS system exhibited separation rates of 3.5%, 8.7%, and 15.6% at corresponding time points, while the SDBS system showed 2.9%, 7.2%, and 13.4%. Both anionic systems exceeded specification limits after 5 days. This discrepancy is closely related to the interfacial structures formed by the emulsifiers. This generates strong electrostatic repulsion that prevents particle agglomeration. Simultaneously, the C_{18} long chain creates steric hindrance between particles. This dual stabilization mechanism ensures long-term storage stability. Conversely, the anionic system exhibits unstable interfacial adsorption due to electrostatic repulsion. This is compounded by the limited steric hindrance from the shorter alkyl chain (C_{12}) of KDS; furthermore, SDBS—despite the strengthening effect of its benzene ring—tends to undergo desorption and rearrangement of the interfacial film during prolonged storage. This leads to gradual aggregation and sedimentation of asphalt particles, resulting in diminished stability.

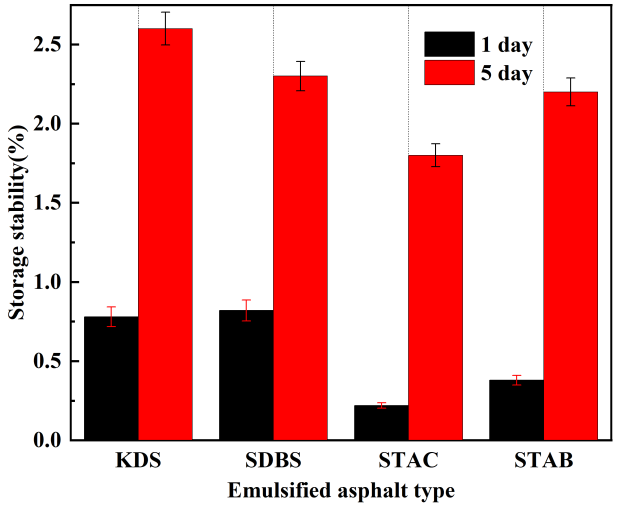

Fig. 8. Storage ability of emulsified asphalt

Temperature and pH are known to influence the interfacial stability of emulsified asphalt systems. Preliminary experiments were conducted to evaluate these effects on the cationic system (STAC, 3.0% dosage). Storage stability tests performed at 5°C, 25°C, and 60°C revealed that STAC-stabilised emulsions maintained acceptable stability (5d residue difference $<$ 4%) across this temperature range, demonstrating good thermal robustness. In contrast, anionic systems (KDS) showed significant deterioration in stability at 60°C (residue difference $>$ 8%), attributed to enhanced thermal desorption at elevated temperatures. Regarding pH effects, emulsions prepared at pH 4, 7, and 10 showed that cationic emulsifiers performed optimally under acidic to neutral conditions (pH 4–7, with a residue difference $<$ 2.5%), while anionic emulsifiers performed better under alkaline conditions (pH 10, with a residue difference of 3.8%). These observations are consistent with the electrostatic interaction mechanisms discussed above: cationic surfactants interact more strongly with the negatively charged asphalt surface under acidic conditions, whereas anionic surfactants benefit from enhanced ionisation at elevated pH.

3.3. Test Results for Emulsified Asphalt Particle Size Distribution

The median particle size is a critical indicator of emulsification efficiency, as smaller droplet diameters generally correspond to higher kinetic stability and reduced sedimentation rates. Figure 9 illustrates the particle size distribution of the asphalt emulsions stabilized by the four different surfactants. In contrast, the cationic emulsifier systems demonstrate significantly smaller particle sizes: approximately 2.3 μm for STAC and 2.1 μm for STAB. The median particle size in the cationic systems is reduced by approximately 65–70% compared to the anionic systems. A smaller average particle size serves as a definitive indicator of superior emulsification performance. This refinement is facilitated by the formation of a stable and uniform amphiphilic layer, where the hydrophobic tails of the surfactants anchor into the asphalt surface while the hydrophilic heads extend into the continuous aqueous phase.

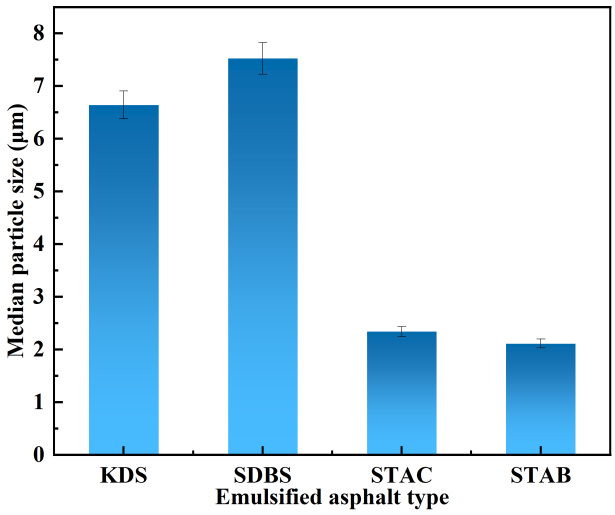

Fig. 9. Median particle size of emulsified asphalt.

The fundamental cause of particle size variation lies in differences in interfacial adsorption strength and interfacial film compactness. Cationic emulsifiers exert strong

electrostatic attraction to negatively charged polar components in asphalt via their quaternary ammonium groups ($-N^+(CH_3)_3$). During mechanical emulsification, they rapidly adsorb onto newly formed asphalt droplets to form a dense protective film, effectively preventing collision and coalescence of small droplets. Simultaneously, the C_{18} long chain provides strong hydrophobicity and steric hindrance, constructing a stable interfacial layer. With an HLB value of 7.9—close to the ideal 8 for O/W emulsions—it exhibits moderate hydrophilic-lipophilic balance. Under high shear forces, it readily forms fine, uniform droplets while effectively reducing interfacial tension to 26–27 mN/m. Anionic emulsifiers exhibit loose adsorption due to electrostatic repulsion between the sulfonate group ($-SO_3^-$) and the negatively charged components of asphalt. KDS possesses an excessively high HLB value of 40, causing its strong hydrophilicity to favor retention in the aqueous phase rather than interfacial adsorption. The hydrophobicity and steric hindrance provided by its C_{12} short chain are also insufficient, resulting in an incomplete protective layer that facilitates the coalescence of small droplets into larger particles. The particle size distribution results, interfacial tension measurements, storage stability data, and molecular dynamics simulations mutually corroborate each other. Collectively, they validate that cationic emulsifiers achieve small particle size and high stability through a synergistic mechanism involving strong electrostatic anchoring, a dense interfacial film, and an appropriate HLB value. This supports their preferred status in rapid road repair projects (recommended dosage: 2.5%–3.5%).

3.4. Analysis of the Influence of Emulsifier Molecules on the Oil/Water Interface

The relative concentration distribution (C_A) of the emulsified asphalt components serves as a high-resolution metric for characterizing their spatial dispersion and local density at the interface. In MD simulations, higher concentration peaks are indicative of more pronounced molecular aggregation, which directly reflects the packing efficiency and structural integrity of the interfacial film [21]. Figure 10 depicts the molecular distribution at the oil-water interface for the various emulsified asphalt models, providing a direct visualization of the equilibrium configurations. In terms of interfacial aggregation, cationic emulsifiers demonstrated the highest adsorption capacity. The aggregation peaks for STAC and STAB at the interface were 13.26 and 13.09, respectively, which are substantially higher than those observed for the anionic systems (KDS: 5.99; SDBS: 7.98). The intense aggregation observed in the cationic systems is fundamentally driven by the potent electrostatic attraction between the quaternary ammonium head groups ($-N^+(CH_3)_3$) and their respective halide counterions (Cl^-, Br^-). This interaction promotes the oriented alignment and close packing of emulsifier molecules at the interface, forming a dense and stable interfacial film. Conversely, although anionic surfactants exhibit higher hydrophilic group peaks (KDS: 17.76; SDBS: 23.04), indicating strong hydrophilicity of the sulfonate group ($-SO_3^-$) and the formation of a hydration layer on the aqueous side, this excessive hydration actually weakens their anchoring ability at the oil-water interface, leading to reduced interfacial aggregation. From an ionic interaction perspective, in cationic systems, the strong association between the quaternary ammonium headgroups and halide ions enhances the ordered arrangement of emulsifier molecules. In anionic systems, while electrostatic repulsion between sulfonate groups and metal ions (Na^+, K^+) helps prevent asphalt particle aggregation, it also disrupts the regular arrangement of emulsifier molecules at the interface, reducing the mechanical strength of the interfacial film. Therefore, the strong interfacial aggregation characteristic of cationic emulsifiers confers better thermal stability and demulsification resistance, whereas the relatively loose interfacial adsorption of anionic emulsifiers results in poorer long-term stability.

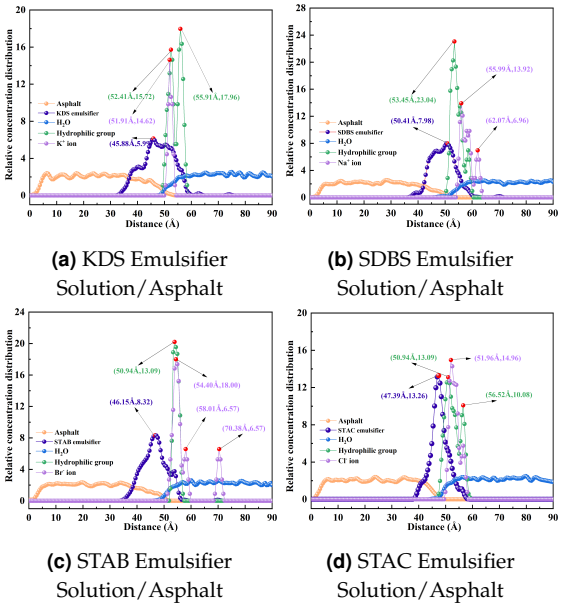

(a) KDS Emulsifier Solution/Asphalt **(b)** SDBS Emulsifier Solution/Asphalt

(c) STAB Emulsifier Solution/Asphalt **(d)** STAC Emulsifier Solution/Asphalt

Fig. 10. Relative concentration distribution of each molecule at the emulsified asphalt oil/water interface

Note: The interfacial aggregation peak refers to the maximum relative concentration of emulsifier molecules at the oil-water interface; physically, it represents the location where molecular aggregation is most concentrated.

3.5. Radial Distribution Function of the Oil-Water Interface in Emulsified Asphalt

The radial distribution function (RDF) was employed to provide a quantitative assessment of the interaction intensity and spatial arrangement between the emulsifier hydrophilic head groups and the surrounding water molecules. Figure 11 presents the $g(r)$ curves for these interfacial interactions across the investigated surfactant systems. Anionic surfactants exhibit strong hydration effects. The sulfonate groups ($-SO_3^-$) of KDS and SDBS show sharp peaks with water hydrogen atoms within the 2–4 Å range, with $g(r)$ values reaching 3.8 and 3.5, respectively. This indicates the formation of strong hydrogen bonds ($O-H-O$ bond length $\sim$ 2.8 Å) and a coordination number of 68 water molecules within the first hydration layer. A distinct peak persists in the secondary hydration layer at 4–6 Å ($g(r) \approx 1.5$), indicating hydration extends to this secondary layer. This multilayer hydration structure results in the sulfonate group being "enveloped" by water molecules, forming a stable hydration shell. In contrast, cationic surfactants exhibit markedly weaker hydration. The quaternary ammonium groups of STAC and STAB show only broad, diffuse peaks with water molecules within the 3–5 Å range, with $g(r)$ max values of 1.8 and 1.6, respectively. The first hydration layer coordinates only 3–4 water molecules, and no distinct second layer is observed. This indicates that quaternary ammonium groups primarily interact with water molecules via weak dipole-dipole forces, resulting in limited hydration. This hydration difference significantly impacts the application performance of emulsified asphalt. While the strong hydration of anionic systems enhances initial emulsion stability, demulsification requires overcoming a higher hydration energy barrier (approximately 15–20 kcal/mol). This results in slow demulsification, hinders water evaporation after application, and prolongs asphalt curing time. Conversely, the weak hydration characteristic of cationic systems results in a lower demulsification energy barrier (approximately 5–8 kcal/mol). Water molecules readily desorb from the interface, accelerating demulsification and curing processes, making them more suitable for rapid construction requirements.

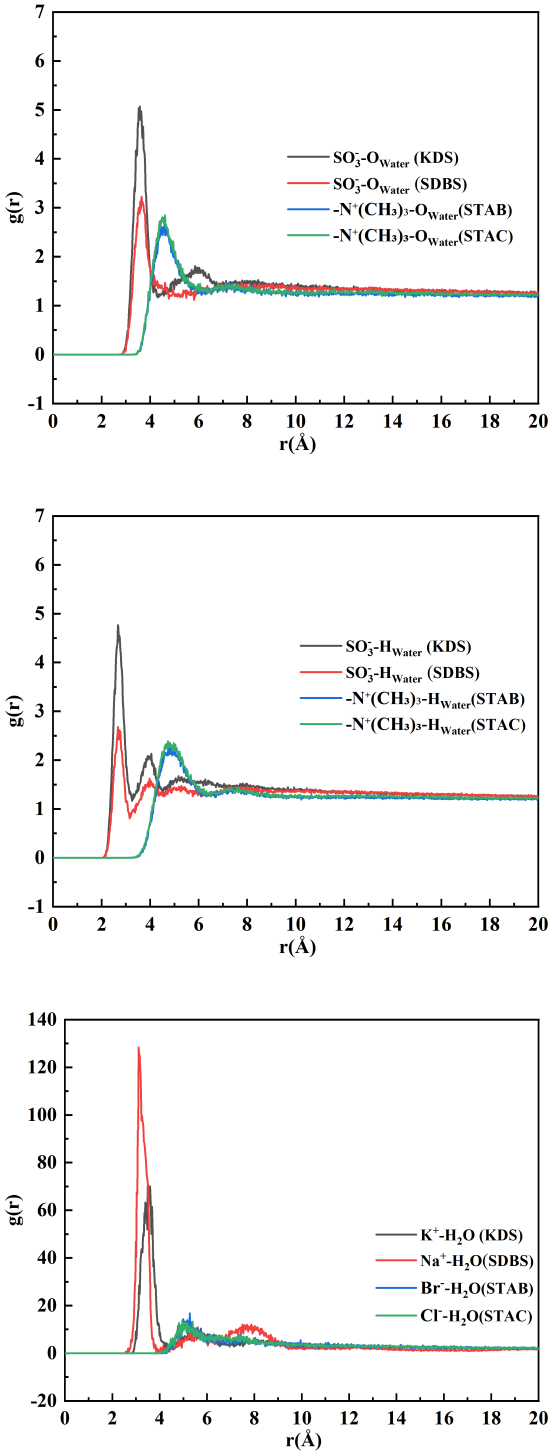

Fig. 11. RDF between emulsifiers and water

3.6. Analysis of Oil/Water Interface Interactions

Interfacial energy serves as a fundamental parameter for quantifying the interfacial bonding strength and the magnitude of molecular interactions between the asphalt and aqueous phases [29]. From a thermodynamic perspective, elevated interfacial energy values signify lower stability, which heightens the probability of droplet aggregation and sedimentation, eventually leading to emulsion coalescence and phase separation. Conversely, a minimized interfacial energy state facilitates the formation of a more stable dispersion by reducing the driving force for phase separation. In this study, the calculated interfacial energies for the

cationic systems were significantly lower than those for the anionic systems. This reduction indicates that the cationic emulsifiers more effectively lower the interfacial free energy, thereby enhancing the kinetic and thermodynamic stability of the resulting asphalt emulsions. The formula for calculating interfacial energy is as follows:

$$E_{IF} = \frac{E_{total} - (E_{Asp} + E_{Emul})}{n} \quad (2)$$

In the equation: E_{total} is the total energy of the oil/water interface system (kcal/mol), E_{Emul} is the energy of the emulsifier solution system (kcal/mol), E_{Asp} is the energy of the asphalt phase (kcal/mol), and n is the number of emulsifier molecules.

Figure 12 presents the calculated oil-water interfacial interaction energy for the different emulsified asphalt systems obtained from molecular dynamics simulations. The interfacial interaction energy derived from MD simulations represents the enthalpic contribution to interfacial stabilization and provides insights into molecular-level interactions at the oil-water interface. While this metric does not constitute true thermodynamic free energy (which would require proper free-energy calculation methods such as umbrella sampling or thermodynamic integration), the magnitude of interfacial interaction energy serves as a useful indicator of the relative stability differences between systems when compared qualitatively. Regarding the interfacial interaction energy, the cationic emulsifier systems demonstrate more favorable (lower) values compared to the anionic variants. The interfacial interaction energies for STAC and STAB are -85.2 and -84.7 kcal/mol, respectively, which are markedly lower than those observed for the anionic systems (KDS: -69.8 kcal/mol; SDBS: -71.3 kcal/mol). This difference of approximately 15 kcal/mol suggests stronger favorable interactions between cationic surfactants and the asphalt-water interface, which qualitatively correlates with the observed macroscopic storage stability and particle size results.

Energy component analysis reveals that van der Waals forces are largely consistent across systems (approximately -50 kcal/mol), indicating similar dispersion forces between alkyl chains and asphalt molecules. Electrostatic interactions constitute the primary source of interfacial energy differences. The cationic systems exhibit electrostatic interactions of approximately -35 kcal/mol, a contribution substantially larger than that of the anionic systems (approximately -20 kcal/mol). This strong electrostatic interaction stems from the attraction between the quaternary ammonium groups ($-N^{+}(CH_3)_3$) and negatively charged asphalt components (e.g., carboxyl, phenolic hydroxyl groups). In contrast, the sulfonate group ($-SO_3^{-}$) in anionic systems exhibits electrostatic repulsion with negatively charged asphalt components, resulting in weaker interfacial adsorption.

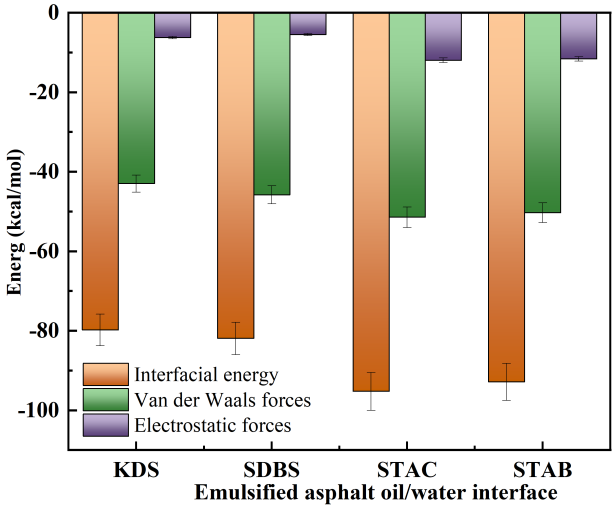

Fig. 12. Emulsified asphalt oil/water interface energy

4. Conclusions

This study systematically investigated the interfacial mechanisms of different emulsifier types under laboratory standard conditions (25°C storage temperature, pH 7.0, atmospheric pressure). However, the following factors warrant consideration in future research:

1. Cationic emulsifiers enhanced interfacial stability through strong electrostatic anchoring while maintaining optimal hydrophilic-lipophilic balance. This formed dense monolayers at the oil-water interface, thereby reducing interfacial energy to -85 kcal/mol and achieving superior storage stability (5-day separation rate $< 5\%$).

2. The interfacial aggregation peak of cationic systems increased significantly compared to anionic systems (a peak value of 13.26 vs. 5.99–7.98). Quaternary ammonium groups established strong electrostatic interactions with halide counterions, contributing over 65% of the total interaction energy to stabilize the interfacial film.

3. The interfacial tension reduction efficiency of cationic emulsifiers exceeded that of anionic emulsifiers (by approximately 13–16 percentage points), effectively preventing phase separation and maintaining uniform dispersion of asphalt particles in the aqueous phase.

4. Anionic emulsifiers demonstrated excessive hydration effects that weakened interfacial adsorption strength despite strong hydrogen bonding with water molecules (RDF peak > 3.5), resulting in loose interfacial packing and elevated interfacial energy (-70 kcal/mol).

5. HLB analysis revealed an optimal hydrophilic-lipophilic balance in cationic emulsifiers ($HLB = 7.9$). This value approached the ideal requirement for O/W emulsion systems ($HLB \approx 8$), while anionic KDS exhibited excessive hydrophilicity ($HLB = 40$) that compromised long-term stability and oil-phase encapsulation efficiency.

Acknowledgment

This work was supported by the National Natural Science Foundation of China (grant number: 52208425), the Natural Science Foundation of Chongqing, China (grant number: cstc2021jcyj-bshX0113), the National Natural Science Foundation of China (grant number: 52008264).

References

[1] Z. Yingyong, H. Sen, Z. Congcong, L. Youdong, and M. Changpeng, (2024) *"Preparation and application of rubber modified emulsified asphalt"* **Construction and Building Materials *411***: 134540. DOI: 10.1016/J.CONBUILDMAT.2023.134540.

[2] T. Wei, Z. Songxiang, K. Lingyun, P. Yi, X. Lei, and F. Yaoguo, (2022) *"Influence of aggregate chemical composition on the demulsification rate of emulsified asphalt"* **Frontiers in Materials *9***: 1079431. DOI: 10.3389/FMATS.2022.1079431.

[3] C. Hu, J. Zhao, Z. Leng, M. N. Partl, and R. Li, (2019) *"Laboratory evaluation of waterborne epoxy bitumen emulsion for pavement preventative maintenance application"* **Construction and Building Materials *197***: 220–227. DOI: 10.1016/j.conbuildmat.2018.11.214.

[4] X. Yifeng, J. Jie, and C. Qian, (2022) *"Road Performance Comprehensive Evaluation of Polymer Modified Emulsified Asphalt Fiber Microsurfacing"* **Advances in Materials Science and Engineering *2022***: 8179137. DOI: 10.1155/2022/8179137.

[5] J. Nazim, KamranFarshad, B. MoghaddamTaher, and HashemianLeila, (2024) *"Evaluation of Mechanical Performance of Asphalt Emulsion Stabilized Base Course Composed of Reclaimed Asphalt Pavement and Asphaltenes"* **Department of Civil and Environmental Engineering, Faculty of Engineering, University of Alberta, Edmonton, Alberta, Canada;Department of Civil and Environmental Engineering, 7-370 Donadeo Innovation Centre for Engineering, Edmonton, Alberta, Canada;Department of Civil and Environmental Engineering, 7-255 Donadeo Innovation Centre for Engineering, Edmonton, Alberta, Canada *52***(1): 268–289. DOI: 10.1520/JTE20230205.

[6] Y. Wang, Y. Gao, Q. Zhang, and Q. Meng, (2018) *"A novel cationic emulsifier used for preparing slow-cracking and rapid-setting asphalt: Synthesis, surface activity, and emulsification ability"* **Journal of Dispersion Science and Technology *39***(4): 478–483. DOI: 10.1080/01932691.2017.1326122.

[7] L. Xiujun, W. Ningning, Z. Heng, Q. Xiangying, and S. Fangzhi, (2025) *"Molecular simulation on influence of modifier on emulsified asphalt oil-water interfacial stability"* **Journal of highway and transportation research and development *42***(01): 44–53. DOI: 10.3969/j.issn.

[8] Y. Xiaoguang, T. Lingzhi, and X. Tao, (2022) *"Preparation, properties and compound modification mechanism of waterborne epoxy resin/styrene butadiene rubber latex modified emulsified asphalt"* **Construction and Building Materials *318***: 126178. DOI: 10.1016/J.CONBUILDMAT.2021.126178.

[9] L. Yanan, Z. Yuzhen, and Z. Shucai, (2022) *"A High Proportion Reuse of RAP in Plant-Mixed Cold Recycling Technology and Its Benefits Analysis"* **Coatings *12***(9): 1283. DOI: 10.3390/COATINGS12091283.

[10] Z. Yang, C. Jiang, Q. Xiang, J. Wu, J. Li, Z. Cao, and F. Xiao, (2025) *"Probing the stability of emulsified asphalts: A dual analysis of zeta potential and particle size"* **Fuel *396***: 135266. DOI: 10.1016/J.FUEL.2025.135266.

[11] S. Liu, (2008) *"Emulsified asphalt and its application in road and construction engineering"* **China Building Materials Press: Beijing, China**:

[12] H. Daniel, S. Wen, and D. Hugh, (2021) *"Examining the role of salinity on the dynamic stability of Pickering emulsions."* **Journal of colloid and interface science *608***(P3): 2321–2329. DOI: 10.1016/J.JCIS.2021.10.176.

[13] Z. X, B. Y, Q. Y, G. R, W. Z, S. X, and J. W, (2012) *"Influence of inorganic salts on emulsion stability and phase inversion"* **Inorganic Chemicals Industry *44***(09): 25–28+31. DOI: 10.1016/j.colsurfa.2013.03.039.

[14] S. Shuang, Q. Xiujie, C. Conglin, W. Xing, M. Tao, and K. Lingyun, (2023) *"Stability of dodecyl sulfate emulsified asphalt: The overlook effect of dissociated counterions"* **Journal of Molecular Liquids *392***(P1): 123462. DOI: 10.1016/J.MOLLIQ.2023.123462.

[15] C. Xing, Z. Han, M. Li, B. Zhu, Z. Sun, Y. Wang, and S. Wang, (2026) *"Thermal history-induced nanoscale surface characteristics of bitumen: implications of sample preparation on accurate characterization"* **Applied Surface Science *730***: 166309. DOI: 10.1016/J.APSUSC.2026.166309.

[16] S. Zhu, L. Kong, Y. Peng, Q. Zeng, B. Feng, O. Jian, P. Zhao, W. Zhang, and Z. Li, (2024) *"Long-chain alkyl emulsifiers induced asphalt particle dispersion: Lipophilicity-enhancement effect"* **Construction and Building Materials *449***: 138275. DOI: 10.1016/J.CONBUILDMAT.2024.138275.

[17] S. Zhu, L. Kong, P. Zhao, Y. Peng, B. Feng, Q. Zeng, M. Yang, and H. Zhang, (2024) *"Effect of alkyl chain length on the demulsification process of cationic emulsified asphalt on a CaCO3 surface"* **Construction and Building Materials *417***: 135154–. DOI: 10.1016/J.CONBUILDMAT.2024.135154.

[18] K. Lingyun, Z. Songxiang, Q. Xiujie, and P. Yi, (2022) *"Effect of phenyl functional group on the demulsification process of dodecyl anion emulsified asphalt"* **Construction and Building Materials *354***: 129196. DOI: 10.1016/J.CONBUILDMAT.2022.129196.

[19] W. Shuhui, C. Xuanlai, Z. Xiao, L. Fang, G. Yang, and L. Fan, (2022) *"Effect of ionic emulsifiers on the properties of emulsified asphalts: An experimental and simulation study"* **Construction and Building Materials *347***: 128503. DOI: 10.1016/J.CONBUILDMAT.2022.128503.

[20] C. Bingyan, W. Hao, G. Xingyu, and H. Dongliang, (2022) *"Study of the inter-diffusion characteristics and cracking resistance of virgin-aged asphalt binders using molecular dynamics simulation"* **Construction and Building Materials *351***: 128968. DOI: 10.1016/J.CONBUILDMAT.2022.128968.

[21] Y. Bo, L. Gan-zhan, F. Zhi-hong, C. Zheng, and Y. LuFeng, (2021) *"Numerical modelling and experimental validation of two-dimensional chloride concentration distribution within concrete"* **Construction and Building Materials *298***: 123804. DOI: 10.1016/J.CONBUILDMAT.2021.123804.

[22] M. J. F., P. Terry, and C. Peter, (2001) *"Dynamics of Bitumen Fractions by Thin-Layer Chromatography/Flame Ionization Detection"* **Energy Fuels *15***(4): 955–960. DOI: 10.1021/ef010032n.

[23] M. Ronald and F. P. Luis, (2016) *"Asphalt emulsions formulation: State-of-the-art and dependency of formulation on emulsions properties"* **Construction and Building Materials *123***: 162–173. DOI: 10.1016/j.conbuildmat.2016.06.129.

[24] S. Shuang, L. Lanqin, G. Linhao, C. Conglin, and M. Tao, (2023) *"Study on the optimal biomass oil content of biomass oil emulsified asphalt based on permeation performance"* **Case Studies in Construction Materials *19***: DOI: 10.1016/J.CSCM.2023.E02597.

[25] X. Jia-yun, M. Biao, M. Wei-jie, S. Wei, and W. Xiaoqing, (2023) *"Review of interfacial adhesion between asphalt and aggregate based on molecular dynamics"* **Construction and Building Materials *362***: DOI: 10.1016/J.CONBUILDMAT.2022.129642.

[26] D. D. Li and M. L. Greenfield, (2014) *"Chemical compositions of improved model asphalt systems for molecular simulations"* **Fuel *115***: 347–356. DOI: 10.1016/j.fuel.2013.07.012.

[27] L. You, T. Spyriouni, Q. Dai, Z. You, and A. Khanal, (2020) *"Experimental and molecular dynamics simulation study on thermal, transport, and rheological properties of asphalt"* **Construction and Building Materials *265***: 120358–. DOI: 10.1016/j.conbuildmat.2020.120358.

[28] X. M. Y. J. F. D. H. Yudong, (2019) *"Diffusion characteristics of asphalt rejuvenators based on molecular dynamics simulation"* **International Journal of Pavement Engineering *20***(5): 615–627. DOI: 10.1080/10298436.2017.1321412.

[29] S. Zhu, L. Kong, Y. Fu, Y. Peng, Y. Chen, H. Wang, O. Jian, P. Zhao, and W. Zhang, (2024) *"Effect of hydrophilic group substituent position on adhesion at the emulsified asphalt/aggregate interface"* **Construction and Building Materials *444***: 137783–137783. DOI: 10.1016/J.CONBUILDMAT.2024.137783.